Formation of Fine B2/β + O Structure and Enhancement of Hardness in the Aged Ti_2AlNb-Based Alloys Prepared by Spark Plasma Sintering

MENGCHEN LI, QI CAI, YONGCHANG LIU, ZONGQING MA, ZUMIN WANG, YUAN HUANG, and HUIJUN LI

Ti_2AlNb-based alloys synthesized at 1223 K (950 °C) by spark plasma sintering were aged at 973 K, 1023 K, 1073 K, and 1123 K (700 °C, 750 °C, 800 °C, and 850 °C), respectively. Phase composition, microstructure, and microhardness of the aged alloys were investigated in this study. Equiaxed O grains and Widmanstätten B2/β + O laths were formed in the aged alloys, and the microhardness was improved in contrast with the spark plasma-sintered alloy without aging. The microhardness relies largely on the O-phase content, as well as the length and width of the O laths. In particular, complete Widmanstätten B2/β + O laths, with locally finely dispersed β precipitates, were obtained in the alloy aged at 1073 K (800 °C), and the alloy exhibited the best microhardness performance. Such fine structure is due to the temperature-dependent transformations $O_{equiaxed} \rightarrow O_{primary}$ + B2/$\beta_{primary}$, $O_{primary} \rightarrow O_{secondary}$ + B2/$\beta_{secondary}$, and B2/$\beta_{primary} \rightarrow O$.

DOI: 10.1007/s11661-017-4193-8

I. INTRODUCTION

Ti_2AlNb-BASED alloys have been used in the aircraft engine due to their low density, high strength, stiffness, oxidation resistance, and outstanding creep resistance.[1–5] According to the lattice structure, the possible phase in the Ti_2AlNb-based alloys includes body-centered cubic (bcc) structured B2 phase (made of two simple cubic lattices shifted by 1/2 the cubic diagonal) or β phase (disordered structure), O (cmcm symmetry Ti_2AlNb) phase, and hexagonal close-packed (hcp) α_2 (DO_{19} structure Ti_3Al) phase.[6] Large Ti_2AlNb ingots are first obtained by smelting or casting from elementary substance of Ti, Al, and Nb, and then processed into desirable shape for application. The multi-phase Ti_2AlNb alloys are likely to experience complicated phase transformation and microstructure evolution during hot working, and fluctuation of the mechanical properties might occur when the large Ti_2AlNb ingots were forged or rolled. In view of this, powder metallurgy was of special interest in recent years, as it has unique advantages in processing metal or ceramic parts with complex shape by filling the powder into a designed mold. Therefore, powder metallurgy is a convenient technique to fabricate well-shaped Ti_2AlNb alloys with less further machining stage. Besides avoiding the waste of metal materials, powder metallurgy could also achieve a certain strength and hardness.[7–9] Hot isostatic pressing (HIP) and spark plasma sintering (SPS) have been used to synthesize Ti_2AlNb-based alloy from elementary powder or from Ti-Al-Nb pre-alloyed powder. Wu *et al.*[8] have studied Ti-22Al-24Nb-0.5Mo alloys prepared by HIP route, and the mechanical properties are largely determined by the HIP temperature and the heat treatment process. Niu *et al.*[9] have prepared powder metallurgic Ti_2AlNb-based alloy by SPS technique at temperatures between 1173 K and 1323 K (900 °C and 1050 °C) with a pressure of 50 MPa. By tailoring the O-phase precipitation within the highly dense B2 matrix, the mechanical properties of the alloys could be controlled. Spark plasma sintering is a pressure-assisted technique, which could improve mass transfer and consolidation to fabricate alloys in high efficiency. It is also a near net shaping technique, and could lead to very fine or ultrafine microstructures exhibiting remarkably high mechanical properties as well.[10]

After bonding the pre-alloyed powder by SPS technique, subsequent heat treatment is required to further tune or regulate the microstructure for favorable

MENGCHEN LI, QI CAI, YONGCHANG LIU, ZONGQING MA, ZUMIN WANG, YUAN HUANG, and HUIJUN LI are with the State Key Lab of Hydraulic Engineering Simulation and Safety, School of Materials Science & Engineering, Tianjin University, Tianjin 300354, PR China. Contact e-mail: licmtju@163.com

Mengchen Li and Qi Cai contributed equally to this work and should be considered co-first authors.

Manuscript submitted December 22, 2016.

Article published online July 5, 2017

properties of the obtained Ti_2AlNb-based alloys. Heat treatment is normally used to strengthen the metal material, reduce the structural weight, and extend the service life of the alloys. Proper heat treatment process can eliminate all kinds of defects caused by the SPS process, refine grains, reduce internal stress, and improve the microstructure and mechanical properties of materials.[11–16] It is therefore essential to understand the microstructure evolution, morphology, and structure–property relationships under various heat treatment processes. Shao *et al.*[11] have observed lamellar α_2/B2 and granular α_2 in the hot-rolled Ti-22Al-25Nb alloy heat treated in both the three-phase and the two-phase region. The phase transformation during the heat treatment was accordingly divided into three stages, including $O \rightarrow \alpha_2 + B2$, $\alpha_2 + O + B2 \rightarrow \alpha_2 + B2$, and $\alpha_2 \rightarrow B2$. For Ti-21Al-29Nb (at. pct) alloys, fully B2 microstructure was obtained when the specimens were aged at temperatures above 1323 K (1050 °C), whereas either equiaxed or Widmanstätten O-phase was found within the B2 grains when aged below 1323 K (1050 °C).[12] The phase evolution and microstructural stability therefore depend largely on the solution and aging temperature. Ti-22Al-20Nb-7Ta cast ingots have been solutionized and aged in B2 + O-phase field, and two kinds of B2→O transformation were observed, including grain size change that is controlled by grain boundary diffusion, and Widmanstätten precipitation of O phase from the B2 matrix.[15] However, previous research has been focused on the relationship between the certain microstructure and the property of the alloys, and the evolution of the microstructure during heat treatment is missing. Also, results have shown that a better O + B2/β microstructure by the aging treatment could result in comprehensive mechanical properties.[17] It is therefore essential to investigate the precipitation of O phase for a homogeneous and refined structure in the Ti_2AlNb-based alloys.

In this study, Ti_2AlNb-based alloys were fabricated from Ti-22Al-25Nb (at. pct) pre-alloyed powder by SPS in α_2 + B2/β + O-phase field. Aging treatment was then carried out in the B2/β + O-phase region with the purpose of acquiring complete B2 + O Widmanstätten structure, and moreover, finely dispersed O particles are expected to precipitate on the B2 matrix. The phase composition and microstructure were investigated at different aging temperatures, and the relationship among the O-phase content, O-phase dimension, and microhardness, was also studied by linear regression. Specially, the microstructure evolution during the aging process was elaborated.

II. EXPERIMENTAL DETAILS

Spherical Ti-22Al-25Nb (at. pct) pre-alloyed powder (single B2 phase, ~235 μm) was sintered at 1223 K (950 °C, *i.e.*, in the α_2 + B2/β + O-phase region) for 10 minutes with the heating rate of 100 K·min^{-1} and with a pressure of 40 MPa by spark plasma sintering technique. Cylindrical Ti_2AlNb-based alloys were obtained with the dimension of Φ 20 × 10 mm after furnace cooling. The as-sintered specimens were then aged in the pipe furnace (SK-G06123K) at 973 K, 1023 K, 1073 K, and 1123 K (700 °C, 750 °C, 800 °C, and 850 °C) for 6 hours (*i.e.*, in the B2/β + O-phase region) followed by furnace cooling, respectively. The phase composition of the Ti_2AlNb-based alloys was measured by X-ray diffraction (XRD, Bruker D8 Advanced) using Cu Kα radiation, and the microstructure of the specimens was characterized by scanning electron microscopy (SEM, Hitachi S-4800) after the alloys were chemically etched with Kroll's reagent. The room-temperature microhardness was examined by the Vickers hardness test (0.2 kg load). In order to confirm the phase transformation and structure evolution during the isothermal process of aging treatment, the as-sintered Ti_2AlNb-based alloys were aged at 1073 K (800 °C) for 0.5, 2, and 4 hours followed by water quenching, and the phase composition and microstructure were characterized as well.

III. RESULTS AND DISCUSSION

Figure 1 illustrates the XRD patterns of pre-alloyed powder, as-sintered Ti_2AlNb-based alloy, and alloys aged at 973 K, 1023 K, 1073 K, and 1123 K (700 °C, 750 °C, 800 °C, and 850 °C) for 6 hours. The Ti_2AlNb-based alloy only solution treated at 1223 K (950 °C) comprised B2 phase and an extremely light amount of O phase, which was identified from the ambiguous peak at around 40 deg in the XRD pattern. As the used pre-alloyed powder was in single B2 phase, the O phase might be originated from the transformation of B2→O. During the following aging treatment, the generously generated O phase became the main phase. Accompanied by the disordering of B2 phase, the aged specimens were composed of O and B2/β phases, which is in accordance with the investigation on the phase transformation in Ti-22Al-25Nb alloys.[4] When the Ti_2AlNb alloys were aged below 1173 K (900 °C), the phase transformation was in the sequence of $B2 \rightarrow B2 + O_{transition} \rightarrow O_{metastability} \rightarrow O + \beta$.[18] This disordering process commonly occurs in the temperature range of 973 K to 1148 K (700 °C to 875 °C), which covers the aging temperature in this study. Figure 1(b) shows the slowly scanned XRD patterns of the Ti_2AlNb-based alloys aged at 973 K, 1023 K, 1073 K, and 1123 K (700 °C, 750 °C, 800 °C, and 850 °C) for 6 hours. The β phase was dominating when the temperature is below 1023 K (750 °C), while the B2 phase emerged when the temperature is above 1023 K (750 °C). This is related to the transformation B2→β, and the phase diagram indicated that order/disorder line for B2/β exists at around 1023 K (750 °C).[19] On the other hand, the phase composition in the aged powder metallurgic specimens differed from that in the Ti_2AlNb ingots, which were composed of α_2, β, and O phases when the aging temperature was 973 K (700 °C).[19] Moreover, the isothermally forged Ti-22Al-25Nb (at. pct) alloy aged in the B2 + O-phase region contained α_2, B2, and O phases as well.[16] In virtue of the high stability of α_2, the transformation $\alpha_2 \rightarrow O$ was inhibited, and dual B2 + O structure was hardly obtained once the

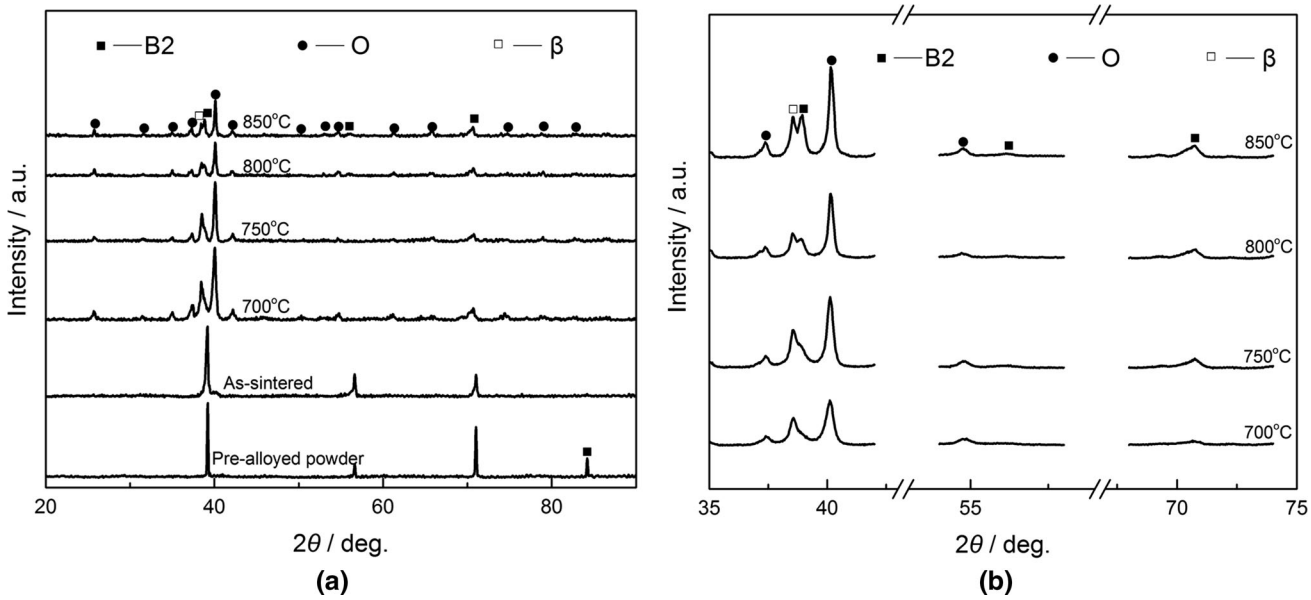

Fig. 1—(*a*) XRD patterns of the as-sintered Ti_2AlNb-based alloy and those aged at 973 K, 1023 K, 1073 K, and 1123 K (700 °C, 750 °C, 800 °C, and 850 °C), and (*b*) XRD patterns of the aged alloys scanned in low speed.

α_2 phase presented in the forged specimens.[20] It seems that the α_2 could be completely removed by powder metallurgy, even though the specimens were solution treated in the α_2 + B2 + O-phase region.

Figure 2 shows the volume percent of the O and B2/β phase in the Ti_2AlNb-based alloys aged at 973 K, 1023 K, 1073 K, and 1123 K (700 °C, 750 °C, 800 °C, and 850 °C). The content was calculated from the peak intensity of the XRD patterns by Rietveld method.[21] The quantitative estimation of phases by X-ray diffraction is based on the principle that the total integrated intensity of all diffraction peaks for each phase is proportional to the volume percent of that phase. Therefore, for the Ti_2AlNb alloys containing B2 phase and O phase, the volume percent of B2, V_{B2}, is written as Eq. [1],

$$V_{B2} = \frac{\sum_{j=1}^{n} \frac{I_{B2}^{j}}{R_{B2}^{j}}}{\sum_{j=1}^{n} \frac{I_{B2}^{j}}{R_{B2}^{j}} + \sum_{i=1}^{m} \frac{I_{O}^{i}}{R_{O}^{i}}}, \quad [1]$$

where *m and n* are the number of examined peaks for O and B2 phase, *R* is the characteristic parameter for each phase.[22]

The content of O phase was considerably increased by aging treatment. The aged samples contained ~70 vol pct O phase, while the as-sintered alloy is composed of almost complete B2 phase. Apart from this, an increasing quantity of O phase was generated when the aging temperature was elevated, and the content reached the maximum at 1073 K (800 °C). This is in agreement with the tendency of the phase content for the specimens sintered in the temperature range of 973 K to 1123 K (700 °C to 850 °C).[23] As dual-phase alloys, the content of B2/β phase revealed a reversed tendency, and was the least at 1073 K (800 °C). Unlike the monotonous increase of O-phase content in the forged Ti-22Al-25Nb alloys when they were aged from

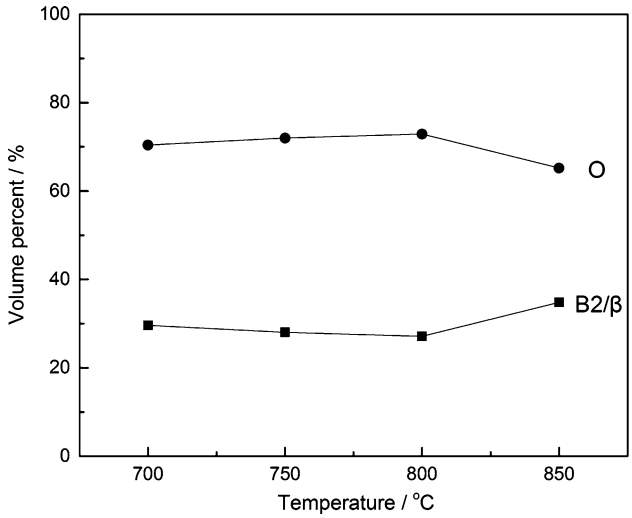

Fig. 2—Phase content of the Ti_2AlNb-based alloys aged at 973 K, 1023 K, 1073 K, and 1123 K (700 °C, 750 °C, 800 °C, and 850 °C).

1033 K to 1113 K (760 °C to 840 °C),[6] the O phase was slightly reduced in the powder metallurgic Ti_2AlNb-based alloys with the increasing aging temperature to 1123 K (850 °C). This temperature has approached the α_2 + B2 phase region, and the O phase began to transform into B2. The phase transformation could be figured out from the published phase diagram.[18,24] The SEM images of the Ti_2AlNb-based alloys aged at 973 K, 1023 K, 1073 K, and 1123 K (700 °C, 750 °C, 800 °C, and 850 °C) are shown in Figure 3. The O phase is present in either equiaxed grains or Widmanstatten laths in the aged specimens, corresponding to the transformation of B2→O and B2→O + B2, respectively. The absence of coarse acicular O indicated that powder metallurgy is conducive to the homogeneity of the microstructure. Furthermore, the

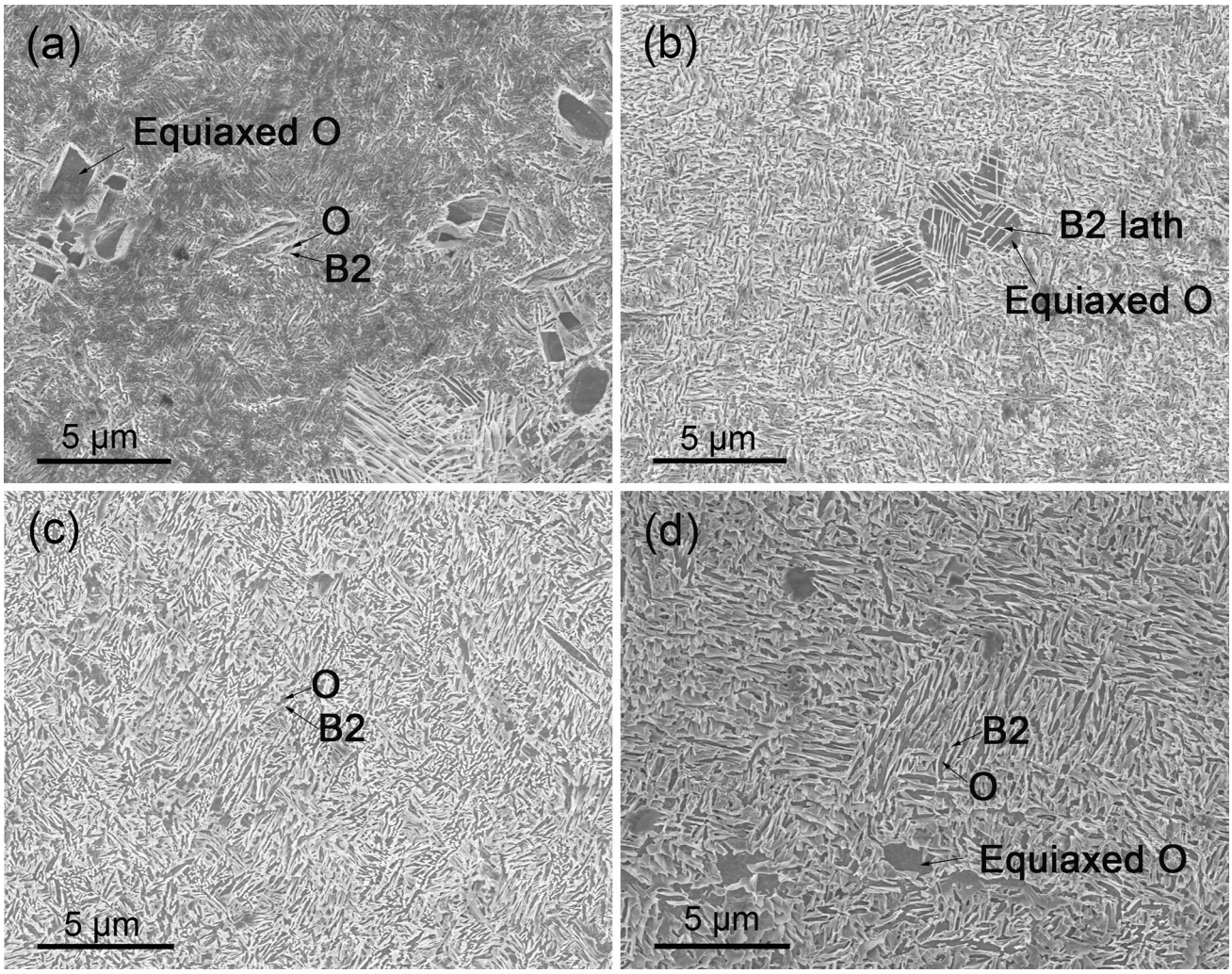

Fig. 3—SEM images of the Ti_2AlNb-based alloys aged at (*a*) 973 K (700 °C), (*b*) 1023 K (750 °C), (*c*) 1073 K (800 °C), and (*d*) 1123 K (850 °C).

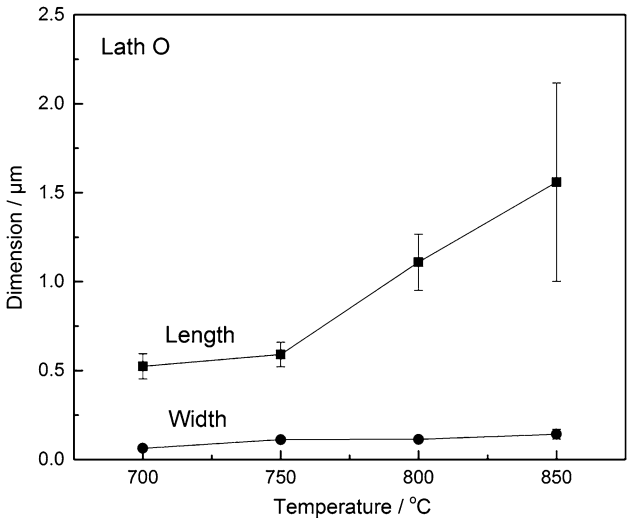

Fig. 4—Length and width of the O laths in the Ti_2AlNb-based alloys aged at 973 K, 1023 K, 1073 K, and 1123 K (700 °C, 750 °C, 800 °C, and 850 °C).

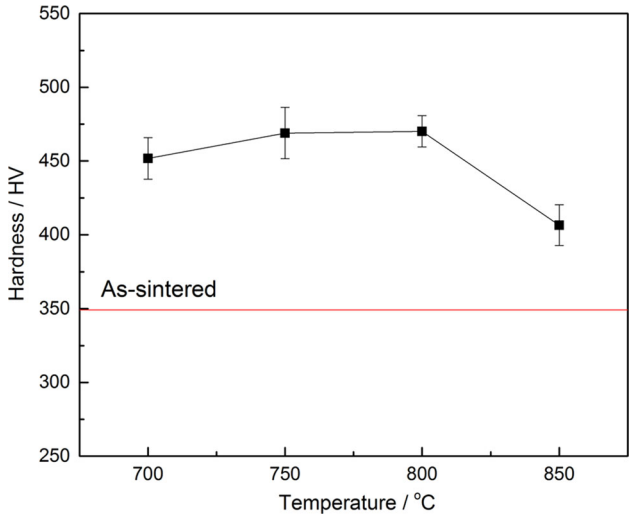

Fig. 5—Vickers hardness of the Ti_2AlNb-based alloys aged at 973 K, 1023 K, 1073 K, and 1123 K (700 °C, 750 °C, 800 °C, and 850 °C).

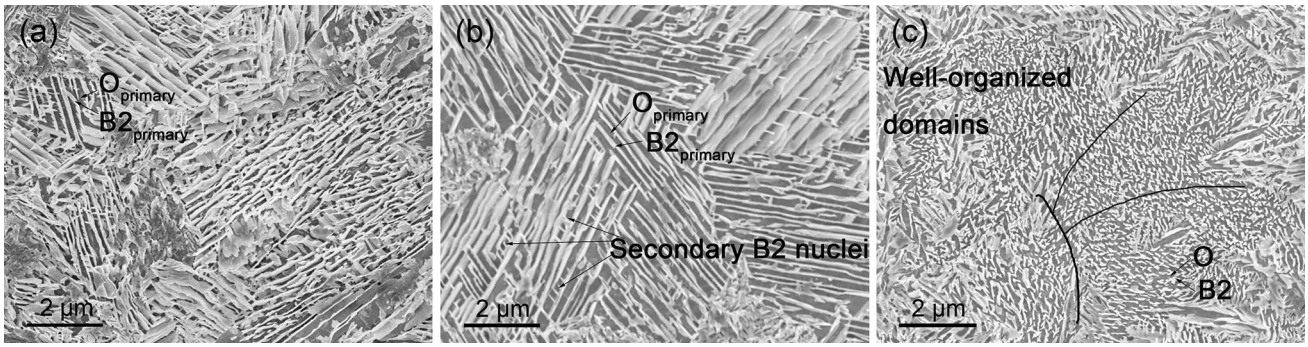

Fig. 6—SEM images of the Ti_2AlNb-based alloys aged at (*a*) 973 K (700 °C), (*b*) 1023 K (750 °C), and (*c*) 1073 K (800 °C).

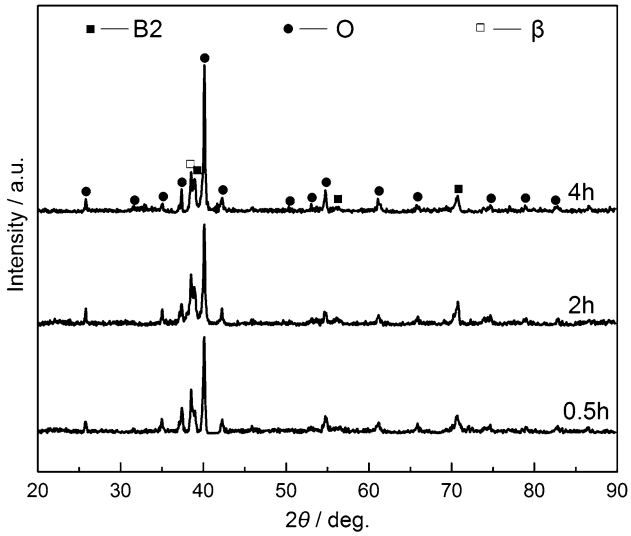

Fig. 7—XRD patterns of the Ti_2AlNb-based alloys aged at 1073 K (800 °C) for (*a*) 0.5 h, (*b*) 2 h, and (*c*) 4 h followed by water quenching.

specimen aged at 1073 K (800 °C), which contained the highest content of O phase, comprised complete B2/β + O Widmanstätten structure, even without equiaxed O phase. This morphology is distinct from the equiaxed α_2 and coarse lath O in the forged Ti-22Al-25Nb alloy solution treated at 1253 K (980 °C) and aged at 1073 K (800 °C).[25] The microstructure evolution with aging temperature could be traced from the SEM images. Within the fine Widmanstätten structure of the specimen aged at 973 K (700 °C), relatively large equiaxed O-phase grains (~3 μm in size) existed in the matrix, and coarse lath colonies have precipitated within some large equiaxed grains, as shown at the right bottom of Figure 3(a). When the aging temperature increased to 1023 K (750 °C), the small equiaxed O grains began to transform into coarse B2 + O lath colonies (Figure 3(b)), and the size of the equiaxed O grains agrees with that in Figure 3(a). Although the equiaxed O grains have been eliminated at 1073 K (800 °C), further elevation of aging temperature to 1123 K (850 °C) led to the reappearance of the equiaxed grains; however, the dimension of the grains was decreased to be about 1 μm.

Along with the size decrease of the equiaxed O grains, the dimension of the Widmanstätten laths, formed from the B2 phase rather than the equiaxed O phase, was increased. The O phase (dark gray area) becomes more visible with the elevated aging temperature as well (Figure 3). The dimension of the lath O in the Widmanstätten structure is measured from the SEM images by Image Pro Plus software 6.0, as shown in Figure 4. Both the measured length and width are increased by more than twice, as the aging temperature increased. The width increased from 0.06 ± 0.01 μm for specimen aged at 973 K (700 °C) to 0.14 ± 0.03 μm for that aged at 1123 K (850 °C), and the length increased from 0.52 ± 0.07 to 1.56 ± 0.56 μm. Nevertheless, the dimension is less than that (~2.6 μm in length and 0.8 μm in width for lath O) in the forged alloy solution treated in the three-phase region and aged in the B2/β + O region.[16] In this regard, the Widmanstätten structure is refined in the powder metallurgic Ti_2AlNb alloys.

Figure 5 shows the room-temperature microhardness of Ti_2AlNb alloys aged at 973 K, 1023 K, 1073 K, and 1123 K (700 °C, 750 °C, 800 °C, and 850 °C). For starters, the hardness has been improved by aging treatment, in contrast with the as-sintered alloys by SPS (349 ± 11 HV). Except for the severe decrease at 1123 K (850 °C), the Vickers microhardness shows similar variation tendency to the O-phase content, as the aging temperature elevated. In view of this, the size of the Widmanstätten lath of O phase is measured to interpret the hardness performance as well, while the equiaxed grains have been found to have little influence on the microhardness.[16,26] Using linear regression analysis, the relationship between the microhardness and the O phase is verified. The multiple linear regression equation can be defined as follows.[16]

$$Y_{\text{microhardness}} = b_0 + b_1 V_{\text{O}} + b_2 L_{\text{LathO}} + b_3 W_{\text{LathO}}, \quad [2]$$

where b_0, b_1, b_2, and b_3 represent the multiple linear regression parameters. The relationship between microhardness and O phase is written as $Y_{\text{microhardness}} = 336.10 + 2.22\, V_{\text{O phase}} - 65.96\, L_{\text{Lath O}} + 247.10\, W_{\text{Lath O}}$ according to Eq. [2]. The regression parameters are in the same order as those in Wang's study,[16] and the correlation coefficient of the regression, R^2, is 0.9368. Returned to the tendency of the hardness, it increased gently from 973 K to 1073 K (700 °C to 800 °C), with the maximum of 470 ± 10 HV, and then sharply decreased at 1123 K (850 °C), with the lowest value of

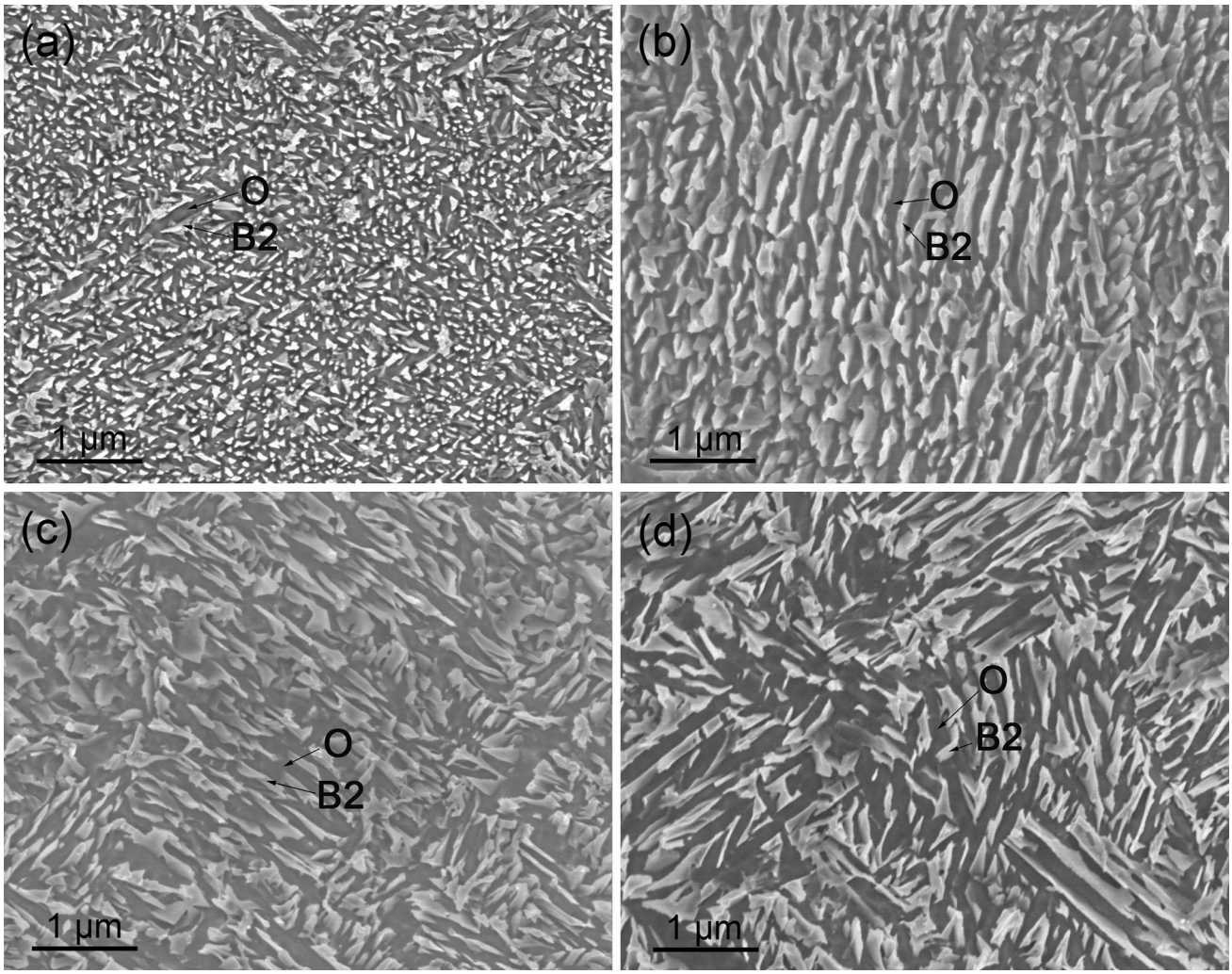

Fig. 8—SEM images of the Ti_2AlNb-based alloys aged at 1073 K (800 °C) for (*a*) 0.5 h, (*b*) 2 h, (*c*) 4 h, and (*d*) 6 h.

406 ± 13 HV. Such tendency is inconsistent with the monotonic decrease of hardness in the forged alloy solution treated in three-phase region and aged from 1033 K to 1113 K (760 °C to 840 °C).[16]

The highest hardness is obtained when the aging temperature is 1073 K (800 °C), and this specimen contains complete B2/β + O Widmanstätten microstructure without visible equiaxed O grains. However, one could distinguish finely dispersed B2/β + O area, with the edge as the retained boundary of the equiaxed O grains, from the matrix. The size of this B2/β + O area is also with the same dimension as the equiaxed grains. Such fine microstructure should be responsible for the enhancement of the hardness. The formation of the fine structure could be traced from the SEM images of the specimens aged below 1073 K (800 °C) (Figure 6). The finely dispersed B2/β + O structure is supposed to generate within the equiaxed O grains, in view of the contours of these grains. When the aging temperature is 973 K (700 °C), B2/β phase began to precipitate as lath colonies within the equiaxed O grains (Figure 6(a)), *i.e.*, $O_{equiaxed} \rightarrow O_{primary}$ + B2/$\beta_{primary}$. The laths are coarser than that precipitated from B2 phase on the matrix. As the aging temperature increases, secondary B2/β nuclei formed between the neighboring laths, *i.e.*, $O_{primary} \rightarrow O_{secondary}$ + B2/$\beta_{secondary}$, with the orientation perpendicular to the primary B2/β laths; however, the growth of the secondary B2/β nuclei is interrupted by the primary B2/β laths (Figure 6(b)). For a higher temperature, the primary B2/β laths continued to transform into O phase, B2/$\beta_{primary} \rightarrow$O, and the fine B2/$\beta$ grains were remained in the equiaxed O grains. One could recognize the well-organized domains from Figure 6(c), and the fine grains are in the same orientation within a single domain. Further elevation of the aging temperature led to the solution of secondary B2/β grains, *i.e.*, B2/$\beta_{secondary} \rightarrow O_{equiaxed}$. The equiaxed O grains reappeared on the matrix with a smaller size in contrast with those in the specimen aged at 973 K (700 °C) (Figure 3(a)), and the lath of the lath colonies structure grew instead, as the measured length and width considerably increase when the aging temperature is 1123 K (850 °C) (Figure 4). This process is also known as Ostwald ripening.

To interpret the evolution of such fine microstructure during the aging process, the as-sintered specimens were aged at 1073 K (800 °C) for 0.5, 2, and 4 hours followed by

water quenching, and the XRD patterns are shown in Figure 7. Water quenching is employed to remain the high-temperature phase composition and microstructure to room temperature. The aged specimens are composed of B2/β and O phases, which is the same as the alloys aged at different temperatures followed by furnace cooling, indicating that no B2 or α_2 transformations were involved during the aging process, and only the phase content has been varied. However, the gas-atomized Ti-22Al-27Nb matrix hot rolled in the single-phase region and aged in the B2/β + O region was composed of B2 and O phases.[27] The SEM images of the as-sintered specimens aged at 1073 K (800 °C) for 0.5, 2, 4, and 6 hours are shown in Figure 8. Finely dispersed B2 phase was found in the sample aged for 0.5 hour. As the aging time prolonged, the fine B2 particles began to merge due to the Ostwald ripening, and coarse B2 laths appeared. This process involves the transformation of O→B2, as the peak of B2 phase in the XRD patterns became more intense with the increasing aging time (Figure 7). One could still recognize the edge of the fine B2 particles in the specimen aged for 2, 4, and 6 hours. In this view, aging treatment in Ti_2AlNb-based alloy involves the solution of B2 phase and the uniform of the microstructure.

IV. CONCLUSION

Ti_2AlNb-based alloys, synthesized in α_2 + O + B2 phase region by spark plasma sintering, were aged in B2/β + O phase region in this study. The microhardness was improved for the aged alloys in contrast with the as-sintered one, and in general, the hardness increased first and then decreased with the elevated aging temperature, which agreed with the variation tendency of the O-phase content. The hardness is determined by the O phase content and the dimension of the O laths. The most favorable hardness performance is obtained in the alloy aged at 1073 K (800 °C), since the specimen contained complete B2/β + O Widmanstätten structure with finely dispersed B2/β particles. The fine B2/β particles are generated due to the decomposition of equiaxed O-phase grains and the solution of B2 laths in the O-phase matrix. In contrast with the investigations on forged and welded bulks, powder metallurgy is likely to remove α_2 phase, refine the Widmanstätten structure, and homogenize the microstructure of the Ti_2AlNb-based alloys.

ACKNOWLEDGMENTS

The authors are grateful to the China National Funds for Distinguished Young Scientists (Granted No. 51325401), the National Natural Science Foundation of China (Granted No. 51474156 and U1660201), the National High Technology Research and Development Program of China (Granted No. 2015AA042504) for grant and financial support.

REFERENCES

1. H. Shankar, N.E. Prasad, A.K. Singhand, and T.K. Nandy: *Mater. Sci. Eng. A*, 2006, vol. 424, pp. 71–6.
2. O. Rios, S. Goyel, M.S. Kesler, D.M. Cupid, H.J. Seifert, and F. Ebrahimi: *Scripta Mater.*, 2009, vol. 60, pp. 156–9.
3. J. Kumpfert: *Adv. Eng. Mater.*, 2001, vol. 3, pp. 851–64.
4. J. Kumpfert and C. Leyens: *Structural Intermetallics*, TMS, Warrendale, PA, USA, 1997, pp. 895–904.
5. Y.C. Liu, G.C. Yang, and Y.H. Zhou: *J. Crystal Growth*, 2002, vol. 240, pp. 603–10.
6. K. Muraleedharan, A.K. Gogia, T.K. Nandy, D. Banerjee, and S. Lele: *Metall. Mater. Trans. A*, 1992, vol. 23, pp. 401–15.
7. A. Miklaszewski, M.U. Jurczyk, M. Kaczmarek, A.P. Jaworska, A. Romaniuk, N. Lipinska, J. Zurawski, P. Urbaniak, and M. Jurczyk: *Mater. Sci. Eng. C*, 2017, vol. 73, pp. 525–36.
8. J. Wu, L. Xu, Z.G. Lu, B. Lu, Y.Y. Cui, and R. Yang: *J. Mater. Sci. Technol.*, 2015, vol. 31, pp. 1251–7.
9. H.Z. Niu, Y.F. Chen, D.L. Zhang, Y.S. Zhang, J.W. Lu, W. Zhang, and P.X. Zhang: *Mater. Des.*, 2016, vol. 89, pp. 823–9.
10. M. Tokita: *Mater. Sci. Forum*, 1999, vol. 308, pp. 83–8.
11. B. Shao, Y.Y. Zong, D.S. Wen, Y.T. Tian, and D.B. Shan: *Mater. Charact.*, 2016, vol. 114, pp. 75–8.
12. C.J. Cowen and C.J. Boehlert: *Intermetallics*, 2006, vol. 14, pp. 412–22.
13. T.B. Zhang, G. Huang, R. Hu, and J.S. Li: *Trans. Nonferrous. Met. Soc. China*, 2015, vol. 25, pp. 2549–55.
14. C.J. Boehlert: *J. Phase. Equilib.*, 1999, vol. 20, pp. 101–8.
15. J.H. Peng, S.Q. Li, Y. Mao, and X.F. Sun: *Mater. Lett.*, 2002, vol. 53, pp. 57–62.
16. W. Wang, W.D. Zeng, C. Xue, X.B. Liang, and J.W. Zhang: *Intermetallics*, 2014, vol. 45, pp. 29–37.
17. S.R. Dey, S. Suwas, J.J. Fundenberger, and R.K. Ray: *Intermetallics*, 2009, vol. 17, pp. 622–33.
18. C.J. Boehlert, B.S. Majumdar, V. Seetharaman, and D.B. Miracle: *Metall. Mater. Trans. A*, 1999, vol. 30, pp. 2305–23.
19. O.G. Khadzhieva, A.G. Illarionov, and A.A. Popov: *Phys. Met. Metallogr.*, 2014, vol. 115, pp. 12–20.
20. K. Muraleedharan, D. Banerjee, S. Banerjee, and S. Lele: *Phil. Mag.*, 1995, vol. 71, pp. 1011–36.
21. H.M. Rietveld: *J. Appl. Cryst.*, 1969, vol. 2, pp. 65–71.
22. A.K. De, D.C. Murdock, M.C. Mataya, J.G. Speer, and D.K. Matlock: *Scr. Mater.*, 2004, vol. 50, pp. 1445–9.
23. A.A. Popov, A.G. Illarionov, S.V. Grib, S.L. Demakov, M.S. Karabanalov, and O.A. Elkina: *Phys Met. Metallogr*, 2008, vol. 106, pp. 399–10.
24. U.R. Kattner and W.J. Boettinger: *Mater. Sci. Eng. A*, 1992, vol. 152, pp. 9–17.
25. W. Wang, W.D. Zeng, C. Xue, X.B. Liang, and J.W. Zhang: *Intermetallics*, 2015, vol. 56, pp. 79–86.
26. H.N. Wu, D.S. Xu, H. Wang, and R. Yang: *J. Mater. Sci. Technol.*, 2016, vol. 32, pp. 1033–42.
27. S. Emura, M. Hagiwara, and S.J. Yang: *Metall. Mater. Trans. A*, 2004, vol. 35A, pp. 2971–79.